Sparse Power Angle Spectrum Estimation

Jon W. Wallace, *Member, IEEE*, and Michael A. Jensen, *Fellow, IEEE*

***Abstract*—A novel method for estimating the power angle spectrum (PAS) is presented that decomposes the true PAS into a small set of basis functions. The basis coefficients for this sparse representation are found by enforcing equality to the covariance or Bartlett PAS subject to a minimum ℓ_1-norm constraint. The method, referred to as sparse PAS estimation (SPASE), can be implemented conveniently using existing linear-programming (LP) solvers. Further, because only a few clusters are required in the representation, the method enables reduced-complexity stochastic models for the channel and possibly allows reduced overhead in channel feedback schemes. Application of the method to simulated channels and multiple-input multiple-output (MIMO) propagation data demonstrates the utility of the method.**

***Index Terms*—Direction of arrival estimation, modeling, multipath channels, multiple-input multiple-output (MIMO) systems.**

I. Introduction

THE power angle spectrum (PAS) of transmitted or received electromagnetic waves quantifies the relative propagating power as a function of angle at a specific point in space. Traditionally PAS is a single-directional single-polarization quantity, but straightforward double-directional, multi-polarization, and joint azimuth/elevation extensions are also possible. Although we focus on estimating PAS for wireless communications and directional channel modeling, knowledge of the PAS is useful in many other applications, such as radar, radioastronomy, and spaceborne microwave imaging, indicating targets, emissive sources, scatterers, etc.

PAS can theoretically be measured with a directional antenna that is rotated to sense the incoming power (or to transmit power) in a single direction, but this arrangement is often too bulky, expensive, and slow for most applications. For directional wireless channel modeling, a number of techniques have been developed and employed to estimate PAS conveniently from multiple-antenna measurements. Beamforming [1] is a typical method to estimate PAS directly from the array channel response, with the main restrictions being the resolution limitation and existence of side lobes created by the finite array aperture that can be partially overcome by applying deconvolution techniques [2]–[5].

The resolution limitation of traditional methods has been overcome by a parametric description of the channel, where the channel is assumed to consist of a discrete sum of propagating plane waves, referred to commonly as the double-directional channel [6]. The directions and amplitudes of the propagating waves are estimated using super-resolution techniques, such as CLEAN, ESPRIT, SAGE and their variants [2], [7], [8], from which the PAS can easily be extracted. A difficulty of applying these techniques is the need for very accurate array calibration [9], which may not be possible in practice. It has also been shown that when too many multipath arrivals are present, the PAS estimated using these super-resolution techniques can be highly inaccurate [10].

For many applications it is desirable to find an accurate PAS representation with as few parameters as possible, referred to as a sparse representation (or "simplest explanation" according to Occam's Razor). For directional channel modeling, 10 s to 100 s of multipath can be grouped into relatively few clusters, simplifying the stochastic model. From the standpoint of channel feedback, passing fewer parameters between nodes is preferable for conserving valuable bandwidth. Related is a growing body of work on signal processing techniques that provide sparse representations of signals and operators using redundant dictionaries [11]–[13].

The purpose of this paper is to present a novel technique for PAS estimation that is both accurate and sparse, which we refer to as sparse power angle spectrum estimation (SPASE). Some aspects of the method have already been presented in [14]–[16], but a complete description has not yet appeared. The method is based on minimum ℓ_1-norm representations of the PAS, which have been shown to produce very sparse representations of signals and operators [11], in contrast to minimum ℓ_2-norm solutions. The method requires no special array or antenna geometry and is quite general. The technique is relatively simple to implement, since linear programming (LP) functions are available in most commercial mathematical software packages. It should be noted that the goals of this method are similar to those of other methods that have been proposed for cluster estimation [10] and estimation of arrivals with finite angular spread [17], [18].

In this development, $\mathbf{A}$ and $\mathbf{x}$ represent a matrix and vector, respectively, with scalar elements a_{ij} and x_i. Matrix conjugate, transpose, and conjugate transpose are represented with $\{\cdot\}^*$, $\{\cdot\}^T$, and $\{\cdot\}^H$, respectively. $\mathcal{A}$ is an Nth order tensor with elements $a_{i_1 i_2 \ldots i_N}$ and $i_\ell \in \{1, \ldots, I_\ell\}$. The tensor $\mathcal{A}$ may be reshaped into a matrix $\mathbf{A}$ with elements $a_{[i_1 i_2 \ldots i_M][i_{M+1} \ldots i_N]} = a_{k_1 k_2}$ where the indices in brackets denote stacking, meaning $k = [i_1 i_2 \ldots i_N]$ denotes $k = \sum_{n=1}^{N} (i_n - 1) \prod_{m=1}^{n-1} I_m + 1$, which is exactly the row-order stacking operation that occurs in mathematical software like MATLAB. A repeated index not appearing on the left-hand side of an equation implies summation, so a matrix-vector multiply could be written as $y_i = a_{ij} x_j \equiv \mathbf{y} = \mathbf{A}\mathbf{x}$. The inner product of two tensors is denoted $\langle \mathcal{A}, \mathcal{B} \rangle = a_{i_1, i_2, \ldots, i_N} b^*_{i_1, i_2, \ldots, i_N}$. The outer product of an Nth order tensor

Manuscript received February 12, 2008; revised January 03, 2009. First published June 05, 2009; current version published August 05, 2009.

J. W. Wallace is with the School of Engineering and Science, Jacobs University Bremen, 28759 Bremen, Germany (e-mail: wall@ieee.org).

M. A. Jensen is with the Department of Electrical and Computer Engineering, Brigham Young University, Provo, UT 84602 USA (e-mail: jensen@ee.byu.edu).

Digital Object Identifier 10.1109/TAP.2009.2024465

$\mathcal{A}$ and an Mth order tensor $\mathcal{B}$ is $\{\mathcal{A} \circ \mathcal{B}\}_{i_1 i_2 \ldots i_N j_1 j_2 \ldots j_M} = a_{i_1 \ldots i_N} b_{j_1 \ldots j_M}$.

II. Sparse Decomposition Methods

Providing a comprehensive survey of sparse decomposition methods and algorithms is beyond the scope of this present work. However, including some background material on the development of this interesting field is important to place the current work in the proper context, indicating room for improvement in the efficiency and utility of the described methods and highlighting future research opportunities to apply sparse decompositions to new antennas and propagation topics. Sparse decomposition aims to solve [12]

$$\min \|\mathbf{x}\|_0 \quad \text{subject to} \quad \mathbf{Z}\mathbf{x} = \mathbf{y} \tag{1}$$

where $\|\mathbf{x}\|_p$ is the ℓ_p-norm of $\mathbf{x}$, defined as $\|\mathbf{x}\|_p = (\sum_i |x_i|^p)^{1/p}$. The special cases $\|\mathbf{x}\|_0$ and $\|\mathbf{x}\|_\infty$ give the number of nonzero elements and the maximum element magnitude, respectively. Typically $\mathbf{y}$ is an observed quantity to be decomposed into a sum of basis vectors given by the columns of $\mathbf{Z}$ with corresponding basis coefficients $\mathbf{x}$. The interpretation of (1) is that the sparsest decomposition is the one with the fewest nonzero coefficients that matches an observation. With noisy signals or an imperfect model, the equality constraint in (1) cannot be strictly met, and the modified problem

$$\min \|\mathbf{x}\|_0 \quad \text{subject to} \quad \|\mathbf{Z}\mathbf{x} - \mathbf{y}\|_p \le \rho_p \tag{2}$$

is usually considered. The choice of p depends on the specific notion of "close" for a given application, and ρ_p provides a tradeoff between the solution sparseness and accuracy.

One of the oldest examples of sparse decomposition methods is the so-called CLEAN algorithm used extensively in radioastronomy [2], in which the observed scene consists of a small set of point sources convolved with the radiation patterns of the receiving antenna(s). One-dimensional CLEAN is described by (2), where y_i, $\mathbf{z}_i$ (ith column of $\mathbf{Z}$), and x_i are the observed signal, antenna pattern, and point source amplitude at the ith scan angle. CLEAN successively detects peaks in the observed scene and subtracts the antenna pattern centered at each peak, resulting in a sparse deconvolved image of relatively few impulses. CLEAN-like algorithms have also been referred to as "matching pursuit" [19]. Although efficient and simple, a drawback of CLEAN is residual error at each step, leading to artifacts and missed sources.

In [20], a synthesis method for sparse arrays is presented, where given the desired pattern, aperture, and allowed deviation from the ideal pattern, a minimum ℓ_p norm decomposition yields the sparsest representation with $0 < p < 1$, and a solution method similar to LP was employed.

In the methods described so far, the single basis used for reconstruction is dictated by the physical antenna pattern. In other problems, the basis is arbitrary and should be chosen to enhance the sparseness of the resulting decompositions. In [11], the concept of atomic decomposition with "basis pursuit" is introduced, where the difficult problem (2) is replaced with

$$\min \|\mathbf{x}\|_1 \quad \text{subject to} \quad \|\mathbf{Z}\mathbf{x} - \mathbf{y}\|_p \le \rho_p. \tag{3}$$

For $p = 1$ or $p = \infty$, and real-valued $\mathbf{x}$, $\mathbf{y}$, and $\mathbf{Z}$, (3) can be solved via LP, which in standard form solves

$$\hat{\mathbf{x}} = \arg\min \mathbf{c}^T\mathbf{x} \quad \text{subject to} \quad \begin{matrix} \mathbf{y} = \mathbf{Z}\mathbf{x} \\ x_i \ge 0 \ \forall i. \end{matrix} \tag{4}$$

Basis pursuit also embraces the idea that $\mathbf{Z}$ may consist of an "overcomplete" or redundant basis whose members need not be linearly independent, further enhancing the potential sparseness of the solution. A rigorous mathematical treatment is given in [12], providing necessary conditions where the solution to (3) for $p = 1, 2$ is also the solution to (2).

More recently, work has appeared on applying sparse representations for image denoising [13], where dictionaries are learned by finding sparse reconstructions of sub-images from a redundant discrete cosine transform (DCT) basis.

An important effort is the search for fast implementations of sparse decomposition techniques. For example, in [21], [22] an efficient iterative algorithm for solving (3) with $p = \infty$ is described. Instead of the normal procedure of iterating on $\mathbf{x}$ to find the optimal solution, the dual problem

$$\max_{\mathbf{d}} \mathbf{y}^T\mathbf{d} - \rho_\infty \|\mathbf{d}\|_1 \quad \text{subject to} \quad \|\mathbf{Z}^T\mathbf{d}\|_\infty \le 1 \tag{5}$$

is solved, where the number of nonzero elements of $\mathbf{x}$ is searched from $1 \ldots N$, and at each step, ρ_∞ must fall within an interval that can be directly computed. The iteration stops when the target value of ρ_∞ falls in that interval. This fast algorithm requires at most N steps, which can be more efficient than standard LP methods.

III. Sparse Power Angle Spectrum Estimation

This section provides details of the SPASE method. We initially describe the method for the single-dimensional case (i.e. single-directional, single-polarization, azimuth-only), and later show how to naturally extend the method to higher dimensions. Although it is likely that improvements in efficiency are possible by applying more sophisticated techniques such as those in [21], this present work focuses on developing the method in a framework compatible with conventional LP solvers that are readily available in most standard mathematical software.

A. Channel Statistics

Consider a system with a single transmit antenna and N_R receive antennas. Assuming L discrete multipath arrivals (L can be arbitrarily large), the narrowband channel transfer function for the ith receive antenna can be written as

$$h_i = \frac{1}{\sqrt{L}} \sum_{\ell=1}^{L} \alpha_\ell g_i(\phi_\ell) \tag{6}$$

where α_ℓ is the complex amplitude of the ℓth path, $g_i(\phi) = e_i(\phi)\exp[j\psi_i(\phi)]$ is the ith element of the steering vector, $e_i(\phi)$ is the complex azimuthal far-field radiation pattern for the ith

antenna, $\psi_i(\phi) = k_0(x_i \cos\phi + y_i \sin\phi)$, x_i and y_i are the coordinates of the ith antenna, and k_0 is the wavenumber. The channel covariance is

$$r_{ik} = \mathrm{E}\{h_i h_k^*\} = \frac{1}{L}\sum_{\ell_1=1}^{L}\sum_{\ell_2=1}^{L}\mathrm{E}\left\{\alpha_{\ell_1}\alpha_{\ell_2}^*\right\}\mathrm{E}\left\{g_i(\phi_{\ell_1})\, g_k^*(\phi_{\ell_2})\right\} \quad (7)$$

where independence of the arrival amplitudes and directions is assumed. If the arrival amplitudes are i.i.d. and zero mean,

$$\mathrm{E}\left\{\alpha_{\ell_1}\alpha_{\ell_2}^*\right\} = F(\phi_{\ell_1})\,\delta_{\ell_1\ell_2} \quad (8)$$

where $F(\phi)$ is the expected power of an arrival in the ϕ direction. This result leads to

$$r_{ik} = \frac{1}{L}\sum_{\ell=1}^{L}\int_0^{2\pi} d\phi_\ell f(\phi_\ell) F(\phi_\ell) g_{ik}(\phi_\ell) \quad (9)$$

$$g_{ik}(\phi) = e_i(\phi) e_k^*(\phi)\exp\{j[\psi_i(\phi) - \psi_k(\phi)]\} \quad (10)$$

where $f(\phi)$ is the probability density function (pdf) of multipath arrivals. Defining $p(\phi) = f(\phi)F(\phi)$ as the *true PAS* and assuming i.i.d. arrivals, (9) becomes

$$r_{ik} = \int_0^{2\pi} d\phi p(\phi) g_{ik}(\phi). \quad (11)$$

The development above can naturally be extended to higher dimensions, where the tensor notation is convenient. Given arrays at both transmit and receive, the relationship becomes

$$r_{i_1k_1i_2k_2} = \int_0^{2\pi} d\phi_R \int_0^{2\pi} d\phi_T p(\phi_R, \phi_T) g_{i_1k_1i_2k_2}(\phi_R, \phi_T) \quad (12)$$

with $\mathcal{G} = \mathbf{a}_R(\phi_R) \circ \mathbf{a}_T(\phi_T) \circ \mathbf{a}_R^*(\phi_R) \circ \mathbf{a}_T^*(\phi_T)$, and $\mathbf{a}_P$ is the single-directional steering vector with $P = T$ (for transmit) or $P = R$ (for receive). For multiple independent polarizations, (11) can be extended to

$$r_{ik} = \int_0^{2\pi} d\phi p_\nu(\phi) g_{ik\nu}(\phi) \quad (13)$$

where $g_{ik\nu} = e_{i\nu}(\phi) e_{k\nu}^*(\phi)\exp\{jk_0[\psi_i(\phi) - \psi_k(\phi)]\}$, and ν indexes polarization. Similarly, multiple frequency bins and elevation can also be incorporated.

B. Element-Space Solution

Given an estimate of the channel covariance $\hat{\mathbf{R}}$ and considering the relationship (11), our task is to invert the relationship to find a suitable estimate of $p(\phi)$. To accomplish this, we expand the unknown true PAS using N_B basis functions or

$$p(\phi) = \sum_{n=1}^{N_B} a_n d_n(\phi) \quad (14)$$

where $d_n(\phi)$ is the nth basis function. Based on the fact that the PAS represents power (a real, non-negative quantity), it is also desirable that the basis functions $d_n(\phi)$ and coefficients a_n be real and non-negative, thus appealing to physical intuition. Substituting (14) into (13) yields

$$r_{ik} = \sum_{n=1}^{N_B} a_n \underbrace{\int_0^{2\pi} d\phi g_{ik}(\phi) d_n(\phi)}_{q_{ikn}} \quad (15)$$

which can be stacked to obtain

$$r_{[ik]} = \sum_{n=1}^{N_B} q_{[ik][n]} a_n \quad (16)$$

or $\mathbf{r} = \mathbf{Q}\mathbf{a}$. Estimating the a_n using the pseudoinverse is arguably the most obvious way to solve this relationship. However, the resulting power coefficients in $\mathbf{a}$, which should be positive and real, are estimated as complex values in general. The a_n can be forced to be real by splitting real and imaginary parts according to

$$\begin{bmatrix}\mathbf{r}_R \\ \mathbf{r}_I\end{bmatrix} = \begin{bmatrix}\mathbf{Q}_R \\ \mathbf{Q}_I\end{bmatrix}\mathbf{a} \quad (17)$$

which may be written as $\mathbf{r}' = \mathbf{Q}'\mathbf{a}$. Although solving for $\mathbf{a}$ with a pseudoinverse will now yield only real coefficients, they may still be negative. Another problem is that this is a minimum ℓ_2-norm solution that tends to distribute energy among all of the basis coefficients, inconsistent with our desire for a sparse solution.

These difficulties are overcome by solving the real-valued relationship (17) using linear programming (LP) given in (4) with $\mathbf{Z} = \mathbf{Q}'$, $\mathbf{x} = \mathbf{a}$, and $\mathbf{c} = [1 \ldots 1]^T$. The use of LP ensures that power is non-negative and the minimum ℓ_1-norm favors a sparse representation [11].

We have assumed that relation (16) holds exactly when we let $\mathbf{r}$ be a sample covariance matrix, but this may not be possible due to imperfect estimates of $\mathbf{r}$ or imperfect array calibration. We can avoid this difficulty by replacing the strict equality constraint with $\mathbf{r}' = \mathbf{Q}'\mathbf{a} + \boldsymbol{\epsilon}$, and two different methods for treating the residual error are considered: soft and hard limiting.

In the case of soft limiting, $\boldsymbol{\epsilon}$ is assumed to be an unknown quantity to be jointly minimized with $\mathbf{a}$, transforming the minimization problem to

$$\hat{\mathbf{a}} = \arg\min\left(\|\mathbf{a}\|_1 + c_\epsilon\|\boldsymbol{\epsilon}\|_1\right) \quad \text{subject to} \quad \mathbf{r}' = \mathbf{Q}'\mathbf{a} + \boldsymbol{\epsilon}. \quad (18)$$

The choice of residual error cost c_ϵ requires some care. For very high quality data with careful calibration, large values of c_ϵ may be advisable to make the match as close as possible. However, when aberrations are present in the data, forcing such a close match may actually make the model order much higher for only slight improvement in the fit.

Hard limiting constrains $\|\boldsymbol{\epsilon}\|_p$ to be below some threshold ρ_p, identical to (3). In this work, $p = \infty$ has been considered, which constrains the maximum residual to lie below ρ_∞. Although

the choice ρ_∞ also requires care, it appears that hard-limited solutions are less sensitive with respect to ρ_∞ than soft-limited solutions are with respect to c_ϵ.

When enforcing the condition $\mathbf{r}' = \mathbf{Q}'\mathbf{a} + \boldsymbol{\epsilon}$, we may not wish to include all of the rows in this equality for two important reasons: redundancy and uncertainty. First, *redundancy* means that the covariance matrix may contain duplicated information, leading to inefficiency in the LP solution. Consider the Toeplitz covariance matrix for a uniform linear array (ULA). Since only a single row is unique, including all of the covariance matrix elements is wasteful. Second, *uncertainty* implies that elements of the covariance matrix may not be available, or our estimates may be very poor. For example, suppose we form a virtual array with 360° of view by rotating an array of directional patch antennas. We could include the element positions at each rotation as an additional set of virtual array elements. However, if the movement is not precise, the exact phase relationship between elements at different rotations is unknown. Also, consider covariance computation for a ULA. Due to the Toeplitz (shift invariant) structure, we can compute covariance for small antenna spacings with high accuracy by averaging over all appropriate shifts. For large spacings, however, we will have effectively less sample points for covariance computations, which we may wish to exclude. Removing elements from $\mathbf{r}$ that are either redundant or uncertain and discarding the corresponding elements of $\mathbf{Q}'$ and $\mathbf{r}'$ removes equations from the optimization constraints.

The purpose of this discussion is to highlight the flexibility of the method in specifying which covariance elements are matched and how error is constrained. The variant giving an optimal tradeoff between complexity and accuracy likely depends on the application and the quality of the data. Also, future investigations are needed to explore under what conditions each method gives optimal performance.

C. Beamspace Solution

For a large number of sensors (antennas and frequency bins), it may be more efficient to solve the problem in beamspace rather than element space. Any linear transformation of (11) will remain a linear system, where only the values for $\mathbf{Q}$ are transformed. Consider applying a simple Bartlett beamformer to (11), or

$$\begin{aligned} B(\phi) &= \langle \mathbf{G}(\phi), \mathbf{R} \rangle \\ &= \left\langle \mathbf{G}(\phi), \sum_{n=1}^{N_B} a_n \int_0^{2\pi} d\phi' \mathbf{G}(\phi') d_n(\phi') \right\rangle \\ &= \sum_{n=1}^{N_B} a_n \int_0^{2\pi} d\phi' d_n(\phi') \langle \mathbf{G}(\phi), \mathbf{G}(\phi') \rangle . \end{aligned} \tag{19}$$

We can project both sides of (19) onto a set of test functions. Using point matching, we sample both sides at K angles ϕ_k to obtain

$$b_k = B(\phi_k) = \sum_{n=1}^{N_B} a_n \underbrace{\int_0^{2\pi} d\phi' d_n(\phi') \langle \mathbf{G}(\phi_k), \mathbf{G}(\phi') \rangle}_{q_{kn}} . \tag{20}$$

The solution of this equation mirrors that of the element-space equation, except that the dimensionality of $\mathbf{Q}$ will typically be significantly reduced. Also, note that $\langle \mathbf{G}(\phi_k), \mathbf{G}(\phi') \rangle$ is the output of a Bartlett beamformer at look-angle ϕ_k for a plane wave arriving at ϕ', which is a real, non-negative number. Since $d_n(\phi)$ is real and non-negative, the elements of $\mathbf{Q}$ are also real and non-negative.

D. Choice of Basis Functions

The analysis has not yet specified the basis functions used to represent the true PAS. Examples of *unstructured* basis functions are pulse or triangle functions, leading to piecewise constant and piecewise linear PAS, respectively. These unstructured basis functions assume no a-priori information about the source distribution.

On the other hand, a *structured* basis uses functions known to represent the PAS characteristics. For example, in indoor and outdoor environments, it has been observed that each multipath cluster in a PAS has a Laplacian shape [23], [24], suggesting a basis consisting of Laplacian functions with different angular spreads and mean angles. Also, with the LP method, there is no restriction that the basis be orthogonal. If desired, we can form an overcomplete basis that has Laplacian, Gaussian, von Mises, Dirac delta functions, etc., and let the LP solution choose the most sparse representation.

IV. Example Applications

Due to space limitations, it is not possible to explore all facets of the new method, nor to compare it with all other existing methods. Instead, we have chosen to provide a few illustrative examples. First, simulations are used to explore the performance of the method for some ideal cases. Second, application of the method to real multiple-input multiple-output (MIMO) measurements indicates that the method can give meaningful results in even non-ideal situations. In this work, LP solutions are obtained with the freely available PCx package [25]. PCx has the added benefit of operating very efficiently when the coefficient matrix $\mathbf{Z}$ is sparse.

A. Single-Directional SPASE

First, we consider an ideal example to explore some properties of SPASE. Consider a very rich scattering environment where multipath components arrive in Laplacian-shaped clusters with $\sigma = 15°$ angular spread. In this example, the ideal covariance matrix is found by computing the integral (11) numerically with 500 equi-spaced points on the interval $[0, 2\pi]$. The simulated channel is probed with a ULA at the receiver consisting of 0.4λ-separated directional antennas, each having a 3 dB beamwidth of 120° and $\sin\phi$ azimuthal gain pattern. We can obtain 360° of azimuthal view by rotating the array to 3 different positions depicted in Fig. 1.

Fig. 2 depicts the results for two conventional PAS estimation techniques (ESPRIT and the Capon beamformer), where these methods are applied repeatedly to each of the three orientations of the receive array. The true spectrum (solid line) has been generated using a single realization of the single-directional SVA model [26] with parameters $\Gamma = 2$ and $\Lambda = 1$. ESPRIT cannot resolve all arrivals, since the number of multipath components is

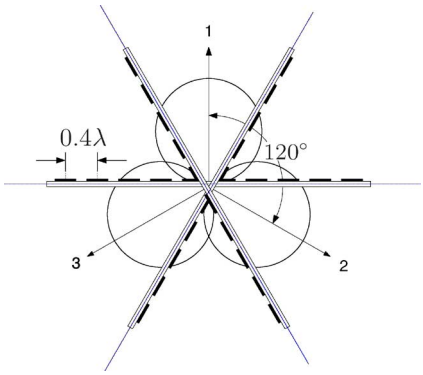

Fig. 1. Directional 8-element array assuming three possible orientations.

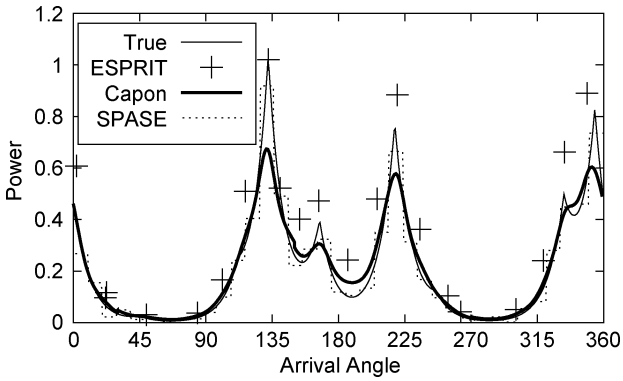

Fig. 2. Example illustrating difficulty of PAS estimation using conventional techniques for environments with rich multipath. Also shown is SPASE with a piecewise-constant basis.

larger than the number of antennas, and the maximum number of 7 arrivals (per orientation) has been chosen as the model order. ESPRIT tends to produce arrivals at the spectral peaks and additional arrivals that mostly follow the PAS shape. However, most of the detail cannot be deduced from the ESPRIT estimates. Although the Capon beamformer gives meaningful results, there is some smoothing of the peaks and smaller arrivals are lost. Also, decomposition of the Capon PAS to a sparse form in terms of clusters would require an additional processing step.

SPASE is now applied to the same example with an unstructured piecewise-constant basis consisting of 36 non-overlapping 10° pulse functions on the interval $[0, 360^\circ]$. Note that for this and following SPASE examples in this section, soft-limiting of the error is used with $c_\epsilon = 1000$. Also, the covariance is normalized by the mean of its diagonal (mean unit power) and the basis functions are normalized to have mean unit power. The result of SPASE is plotted in Fig. 2, indicating a good match for the simple basis assumed.

Fig. 3 shows the results of applying structured SPASE to the same example, where the true cluster arrivals (angle/power) and corresponding true PAS are plotted with boxes and solid lines, respectively. For SPASE, a basis consisting of Laplacian clusters was chosen with angular spreads of $5^\circ, 10^\circ, \ldots, 35^\circ$ and arrival angles of $0^\circ, 2.5^\circ, \ldots, 360^\circ$. Clusters (basis coefficients)

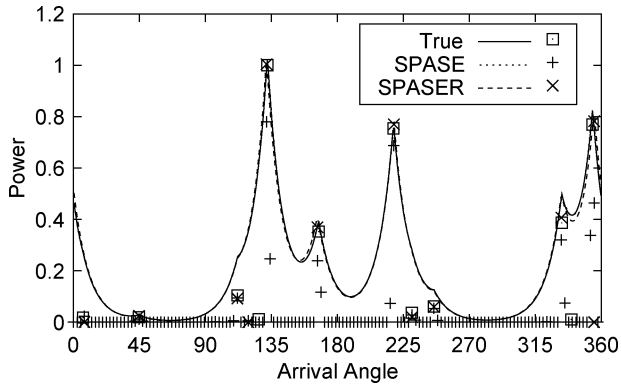

Fig. 3. Example application of SPASE with full basis and a reduced basis (SPASER). Lines represent spectra and symbols represent cluster arrival angle and power.

TABLE I
EXAMPLE RUN-TIMES OF METHODS IN SECONDS

	ESPRIT	Capon	SPASE	SPASER
Total	0.009	0.052	7.078	0.232
Compute $\mathbf{Q}$	–	–	6.066	0.174
LP	–	–	0.927	0.030

and the PAS estimate are plotted as crosses and dotted lines, respectively.

Although the SPASE solution is almost the same as the true PAS, a discrepancy exists between the estimated and actual cluster amplitudes and angles. This problem arises because the actual clusters arrive at angles that are between the specified basis functions, and a nonzero coefficient arises on each side. A reduced basis is obtained by only keeping the basis function with the highest power when two or more adjacent nonzero basis coefficients arise, after which the optimal coefficients are recomputed by rerunning the SPASE algorithm. SPASE with this reduced basis (SPASER) generates cluster arrivals and the PAS estimate shown by X's and the dashed line, respectively. Although the spectrum only changes slightly, the cluster parameters are much closer to the true values.

Due to the higher complexity of the SPASE method compared to simple techniques like ESPRIT or conventional beamforming, knowledge of the added computational burden is of interest. Table I lists the total computational time of the methods in this example in seconds for a laptop with an Intel Core Duo 1.2 GHz processor and 1 GB RAM. Also listed are the portion of time required for computing the $\mathbf{Q}$ matrix and performing LP for SPASE(R). Compared to the sub-second times of ESPRIT or the Capon beamformer, the LP-based SPASE method takes around 7 seconds to complete. Also tabulated is the additional execution time required for SPASER after a SPASE run, which is quite small since very few basis functions are retained. Finally, note that most of the time for SPASE(R) is taken computing numerical integrations for the $\mathbf{Q}$ matrix. This time could be eliminated by using the same $\mathbf{Q}$ matrix from one run to the next or using closed-form solutions for $\mathbf{Q}$ (where possible). Also hybrid techniques might be useful, where candidate basis functions are first identified using the Capon beamformer.

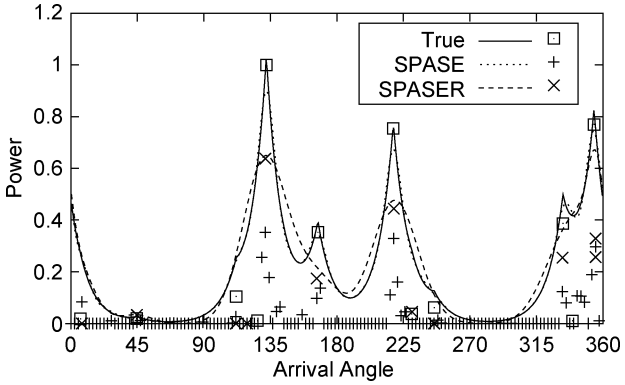

Fig. 4. Example application of SPASE when the actual clusters are Laplacian, but the estimation procedure assumes Gaussian clusters.

So far, we have assumed that both the true PAS clusters and the assumed cluster shapes are the same. Fig. 4 depicts the result when the true clusters are Laplacian, but we assume Gaussian-shaped clusters in the estimation procedure (with the other parameters the same). Notice that SPASE still faithfully represents the PAS, except the peaks are clipped and the representation is not as sparse. When a reduced basis is used, the number of retained clusters is similar to that in the initial case, but the error in the PAS is larger.

These results suggest potential methods for PAS modeling. For example, data could be processed separately with many different basis shapes, and the shape providing the optimal tradeoff between sparseness and low error could then be declared the "true" shape. Another idea is to use a super-basis as suggested in Section III-D and let SPASE choose the most sparse and accurate combination of basis shapes.

B. Unstructured Double-Directional PAS Estimation

This second example considers using an unstructured version of SPASE for double-directional PAS estimation. Such a method could be useful, for example, in ad-hoc networking scenarios, where multi-antenna nodes communicate simultaneously on the same RF spectrum, and the joint PAS is used to avoid interference using space-division multiple access. Sparse estimates of the PAS are desirable, since these would require less transmission overhead.

The beamspace formulation in Section III-C can be extended to the joint MIMO case by letting

$$p(\phi_R,\phi_T)=\sum_{m=1}^{N_{BR}}\sum_{n=1}^{N_{BT}} a_{mn}d_{mn}(\phi_R,\phi_T) \tag{21}$$

where the two-dimensional (2D) pulse functions are

$$d_{mn}(\phi_R,\phi_T)=\begin{cases}1, & \phi_{R,m}-\frac{\Delta\phi_R}{2}\le\phi_R\le\phi_{R,m}+\frac{\Delta\phi_R}{2}\\ & \phi_{T,n}-\frac{\Delta\phi_T}{2}\le\phi_T\le\phi_{T,n}+\frac{\Delta\phi_T}{2}\\ 0, & \text{otherwise}\end{cases} \tag{22}$$

with $\phi_{P,m}=(m-0.5)\Delta\phi_P$ and $\Delta\phi_P=\pi/N_{BP}$.

Analogous to (19), the joint Bartlett spectrum is

$$B(\phi_R,\phi_T)=\langle\mathcal{R},\mathcal{G}(\phi_R,\phi_T)\rangle \tag{23}$$

where $r_{i_1k_1i_2k_2}=\mathrm{E}\{h_{i_1k_1}h^*_{i_2k_2}\}$ and $\mathcal{G}(\phi_R,\phi_T)=\mathbf{a}_R(\phi_R)\circ\mathbf{a}_T(\phi_T)\circ\mathbf{a}^*_R(\phi_R)\circ\mathbf{a}^*_T(\phi_T)$, and $\mathbf{H}$ is the channel transfer matrix. Using point matching on a rectangular grid of K_R and K_T discrete angles at receive and transmit, denoted as $\overline{\phi}_{R,k}$ and $\overline{\phi}_{T,k}$ to obtain $b_{k\ell}=B(\overline{\phi}_{R,k},\overline{\phi}_{T,\ell})$ and making the required substitutions

$$b_{k\ell}=\sum_{m=1}^{N_{BR}}\sum_{n=1}^{N_{BT}} a_{mn}\times\underbrace{\int_0^{2\pi}d\phi_R\int_0^{2\pi}d\phi_T d_{mn}(\phi_R,\phi_T)\left\langle\mathcal{G}(\phi_R,\phi_T),\mathcal{G}(\overline{\phi}_{R,k},\overline{\phi}_{T,\ell})\right\rangle}_{q_{k\ell mn}}. \tag{24}$$

Stacking the dimensions appropriately leads to

$$b_{[k\ell]}=\sum_{[mn]} q_{[k\ell][mn]}a_{[mn]} \tag{25}$$

which is again solved with LP techniques.

In the simulations that follow, full covariance matrices are generated for 100 realizations of the narrowband Saleh-Valenzuela angular (SVA) model [26], assuming Laplacian-shaped clusters with angular spread $\sigma=26^\circ$ at both transmit and receive, unit arrival rate, and decay rate $\Gamma=2$, consistent with measurements of indoor MIMO channels [23]. Arrays at transmit and receive are 8-element ULAs of ideal dipoles with 0.4λ interelement spacing.

For the directional channel model, $N_{BR}=N_{BT}=N_B=12$ with corresponding angles angles $\phi_k=\pi(k-0.5)/N_B$. Note that for the ULA, only angles on one side of the symmetric array need to be considered. The Bartlett spectrum is matched at $K_R=K_T=K=32$ discrete angles given by $\overline{\phi}_k=\pi(k-0.5)/K$.

Fig. 5 plots a single realization of the true spectrum from the SVA model along with the SPASE estimate. Note that soft-limiting of the error is used with the same parameters as in Section IV-A. Although the basic shapes of the spectra are similar, some of the detail is lost due to the stairstep approximation. For this same example Fig. 6 compares the joint Bartlett spectra, indicating that SPASE matches the Bartlett spectra very closely.

The error in the estimated PAS (either true or Bartlett PAS) $\hat{B}$ compared with the actual value B is quantified with

$$\epsilon_B=\frac{\int_0^{2\pi}d\phi_R\int_0^{2\pi}d\phi_T\left|\hat{B}(\phi_R,\phi_T)-B(\phi_R,\phi_T)\right|}{\int_0^{2\pi}d\phi_R\int_0^{2\pi}d\phi_T\left|B(\phi_R,\phi_T)\right|}. \tag{26}$$

Considering the 100 random realizations, average and maximum values of ϵ_B were 0.73% and 2.3% for the Bartlett PAS, respectively, which is considered to be a very good fit. The corresponding average and maximum error in the underlying true PAS were 25% and 37%, respectively, indicating the difficulty of exactly representing sharp Laplacian clusters with the piecewise-constant basis.

The sparseness of the basis decompositions can be judged by how many basis functions were required to capture 90% of

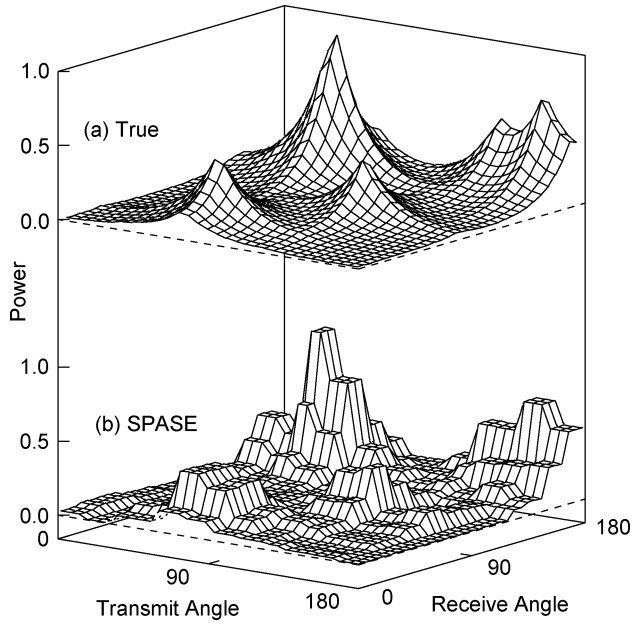

Fig. 5. Comparison of joint double-directional PAS, where (a) is the true PAS generated with the SVA model and (b) is the piecewise-constant SPASE estimate.

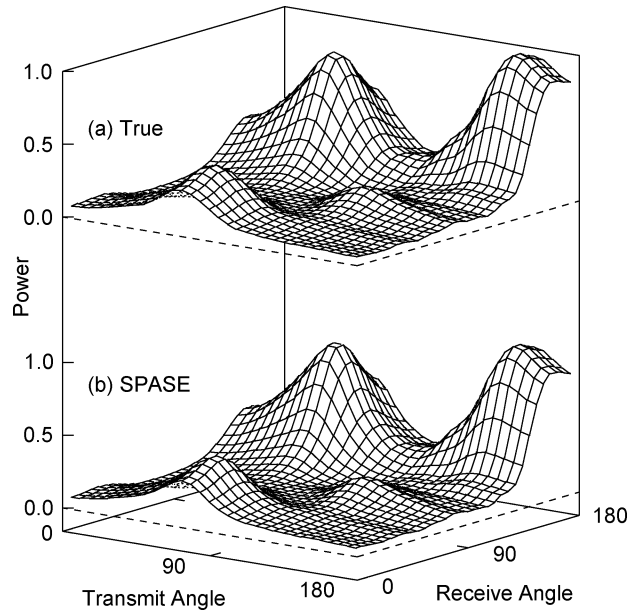

Fig. 6. Comparison of joint double-directional Bartlett PAS for (a) true model and (b) SPASE estimate.

the total energy. For this example, the average and maximum number of basis coefficients was 69 and 114, respectively. This can be compared to the full covariance tensor that has $(8\cdot 8)^2 = 4096$ real parameters.

C. Application to Measured Data

Now we apply the SPASE method to measured indoor wireless data at 5.2 GHz, demonstrating that useful results can be obtained under practical conditions.

1) Channel Measurements: Channel matrices were measured in the electrical engineering building at the Vienna University of Technology at 5.2 GHz [27], [28]. The transmitter consisted of a positionable monopole antenna on a 20 $\times$ 10 xy grid with $\lambda/2$ inter-element spacing. The receiver used a directional 8-element ULA provided by T-Systems Nova GmbH, having 0.4λ inter-element spacing and 3 dB beamwidth of 120°. The channel was probed at $N_F = 193$ equi-spaced frequency bins covering 120 MHz of bandwidth. The transmitter assumed a single fixed location in a hallway. The receive array assumed many different locations in several offices connected to this hallway, as well as three possible orientations: (1) 0° (hallway axis), (2) $-120°$, and (3) $-240°$. The data set for location X and orientation Y is referred to as XDY. The transfer coefficient from the jth transmitter to the ith receiver at the kth frequency for orientation Y is $h_{ij}^{(Y,k)}$.

Transmit covariance $\mathbf{R}_T^{(Y)}$ and receive covariance $\mathbf{R}_R^{(Y)}$ for receive orientation Y were estimated as

$$r_{T,j_1j_2}^{(Y)} = \frac{1}{N_F N_R}\sum_{k=1}^{N_F}\sum_{i=1}^{N_R} h_{ij_1}^{(Y,k)} h_{ij_2}^{(Y,k)*} \tag{27}$$

$$r_{R,i_1i_2}^{(Y)} = \frac{1}{N_F N_T}\sum_{k=1}^{N_F}\sum_{j=1}^{N_T} h_{i_1j}^{(Y,k)} h_{i_2j}^{(Y,k)*} \tag{28}$$

where N_T and N_R are the number of transmit and receive antennas, respectively. To allow 360° of angular view at the receiver, a virtual receive array was created by generating a block diagonal covariance matrix $\mathbf{R}_R = \mathrm{diag}(\mathbf{R}_R^{(1)}, \mathbf{R}_R^{(2)}, \mathbf{R}_R^{(3)})$, where $\mathrm{diag}(\cdot)$ creates a block diagonal matrix from its arguments. Setting off block-diagonal elements to zero is fine, since these equations were pruned during estimation. A single transmit covariance matrix $\mathbf{R}_T$ for 360° of view at the receiver was obtained by averaging the three receive orientations, or $\mathbf{R}_T = (1/3)\sum_{Y=1}^{3} \mathbf{R}_T^{(Y)}$.

Since ULAs were involved in the measurement, we improve covariance estimates by enforcing the shift-invariance condition. Specifically, the shift invariant covariance $\mathbf{R}^{\mathrm{SI}}$ is obtained from the standard covariance $\mathbf{R}$ as

$$R_{ij}^{\mathrm{SI}} = \frac{1}{N_{ij}} \sum_{\{\ell,m:\ell-m=i-j\}} R_{\ell m} \tag{29}$$

where N_{ij} is the number of elements in the sum for the ijth element. After shift invariance is enforced, only a single row of the covariance matrix (per orientation) needs to be retained.

2) Example Location: Next, we show the performance of the new technique and compare to the Capon beamformer. The basis was the same as in Section IV-A. The PAS was estimated separately at transmit and receive to provide better covariance estimates and allow faster convergence of the LP algorithm.

Here, only receive location 9 will be considered. For transmit, a 7 $\times$ 7 element cross array (superposition of two 7-element ULAs) was formed. Spatial smoothing was performed in x and y within a 10 $\times$ 10 grid to improve the covariance estimates. For receive, a virtual 24-element array was formed by considering all orientations as a single array and creating a block diagonal covariance matrix as explained in Section IV-C-1.

When analyzing the data, the element-space solution with hard-limited error was used, since soft-limiting did not work

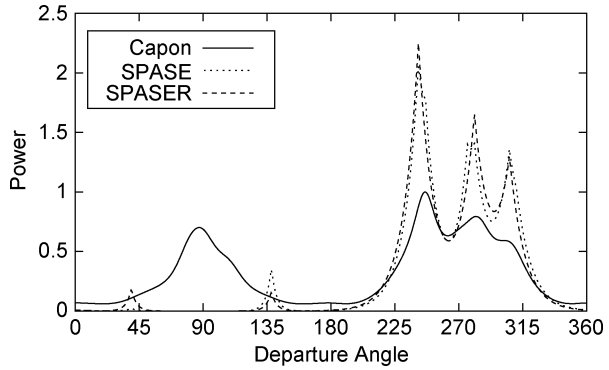

Fig. 7. Estimated transmit PAS for receive location 9 obtained with the Capon beamformer and SPASE.

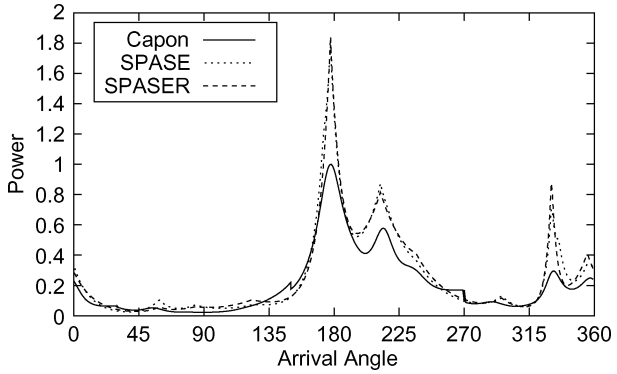

Fig. 8. Estimated receive PAS for receive location 9 obtained with the Capon beamformer and SPASE.

reliably for all scenarios with a fixed c_ϵ. Here, the sample covariances were normalized by the average power (mean of the diagonal), a hard error limit of ± 0.2 was used for the real and imaginary parts, and $c_\epsilon = 5$ (unit error at the limit). These choices seem to provide a good tradeoff between the error and the number of clusters chosen.

Fig. 7 compares spectra obtained with SPASE and the Capon beamformer for the transmit side. The main discrepancy between the Capon beamformer and SPASE occurs in the direction $\theta = 90°$. This artifact appears to be due to aliasing in the endfire directions when element spacing is $\lambda/2$. In other words, the strong energy in the $\theta = 270°$ direction tends to alias into the $\theta = 90°$ direction. Over the range $\theta \in [180°, 360°]$, the Capon beamformer and SPASE look similar, with SPASE providing a sharper response.

Fig. 8 shows the comparison at the receive side. Here, the Capon beamformer has been applied separately to the three ULA orientations, and small discontinuities are present. PAS estimates for Capon's beamformer and SPASE/SPASER have similar trends.

3) Statistical Performance: The goodness of fit of the extracted PAS estimates at the different locations for the transmit and receive covariances is quantified as

$$\epsilon = \frac{||\hat{\mathbf{R}} - \mathbf{R}||_F}{||\mathbf{R}||_F} \tag{30}$$

where $||\cdot||_F$ is Frobenius norm. Over the 24 locations, average and worst-case fractional errors were 15% and 20% for transmit and 17% and 30% for receive, respectively. Also, for four of the 24 locations, the LP solution for the receive PAS estimation failed to find a feasible solution, probably because of the very simple shape used for the antenna reception pattern. The average number of basis functions required to capture 90% of the total energy was only 3.5 for transmit and 4.2 for receive, indicating good sparseness. It should be noted that covariance error appears to be a very sensitive metric, and therefore error around 20% is considered good, especially considering that measured data with imperfect knowledge of calibration and radiation patterns was used.

V. Conclusion

This paper has presented a novel method for power angle spectrum (PAS) estimation based on minimum ℓ_1-norm solutions that can be found numerically with linear programming solvers. The ℓ_1-norm solutions are convenient, since they favor sparse representations, allowing the PAS to be represented with as few basis functions (or clusters) as possible. Sparseness not only allows more tractable models but also may reduce the feedback required for systems that need transmit-side channel state information. The utility of the method was demonstrated by applying the method to both simulated channels and actual MIMO propagation data.

Appendix

In this appendix, details required to transform the minimization problems to LP standard form given in (4) are provided, allowing the methods to be used with most available LP solvers.

In the case of soft-limited error and the element-space solution, standard form requires the unknown $\boldsymbol{\epsilon}$ to be divided into positive and negative error according to $\boldsymbol{\epsilon} = \boldsymbol{\epsilon}_P - \boldsymbol{\epsilon}_M$, so that $\mathbf{r}' = \mathbf{Q}'\mathbf{a} + \boldsymbol{\epsilon}_P - \boldsymbol{\epsilon}_M$. The expanded LP problem becomes

$$\mathbf{y} = \mathbf{r}' \quad \mathbf{x} = \begin{bmatrix} \mathbf{a} \\ \boldsymbol{\epsilon}_P \\ \boldsymbol{\epsilon}_M \end{bmatrix} \quad \mathbf{Z} = [\mathbf{Q}' \quad \mathbf{I} \quad -\mathbf{I}] \tag{31}$$

where $\mathbf{I}$ is the $M \times M$ identity matrix with $M = 2N_R^2$, and N_R is the number of rows or columns in $\mathbf{R}$. The elements of the cost vector become $c_n = 1$ for $1 \le n \le N_B$ and $c_n = c_\epsilon$ otherwise.

For the case of a hard limit on the error, or an ℓ_∞-norm constraint, an LP solution is possible by using the constraint $|\epsilon_i| \le \epsilon_i^{\max}$. Adjusting the constraint to be $-\epsilon_i^- \le \epsilon \le \epsilon_i^+$ and again dividing $\boldsymbol{\epsilon}$ according to $\boldsymbol{\epsilon} = \boldsymbol{\epsilon}_P - \boldsymbol{\epsilon}_M$, we have the constraints $0 \le \epsilon_{Pi} \le \epsilon_i^+$ and $0 \le \epsilon_{Mi} \le \epsilon_i^-$. The LP problem in standard form becomes

$$\mathbf{y} = \begin{bmatrix} \mathbf{r}' \\ \boldsymbol{\epsilon}^+ \\ \boldsymbol{\epsilon}^- \end{bmatrix} \quad \mathbf{x} = \begin{bmatrix} \mathbf{a} \\ \boldsymbol{\epsilon}_P \\ \boldsymbol{\epsilon}_M \\ \mathbf{p} \\ \mathbf{m} \end{bmatrix} \quad \mathbf{Z} = \begin{bmatrix} \mathbf{Q}' & \mathbf{I} & -\mathbf{I} & \mathbf{0} & \mathbf{0} \\ \mathbf{0} & \mathbf{I} & \mathbf{0} & \mathbf{I} & \mathbf{0} \\ \mathbf{0} & \mathbf{0} & \mathbf{I} & \mathbf{0} & \mathbf{I} \end{bmatrix} \tag{32}$$

where $\mathbf{p}$ and $\mathbf{m}$ are vectors of slack variables and $\mathbf{0}$ is a zero matrix. The cost vector is identical to the previous case, except it is padded with zeros (slack variables have zero cost).

ACKNOWLEDGMENT

The authors would like to thank Prof. E. Bonek and the Wireless Communications Group at the Vienna University of Technology in Vienna, Austria for inspiring and substantially improving this work.

REFERENCES

[1] H. Krim and M. Viberg, "Two decades of array signal processing research: The parametric approach," *IEEE Signal Process. Mag.*, vol. 13, pp. 67–94, Jul. 1996.

[2] J. Tsao and B. D. Steinberg, "Reduction of sidelobe and speckle artifacts in microwave imaging: The CLEAN technique," *IEEE Trans. Antennas Propag.*, vol. 36, pp. 543–556, Apr. 1988.

[3] M. A. Richards, "Iterative noncoherent angular superresolution [radar]," in *Proc. IEEE National Radar Conf.*, Apr. 20–21, 1988, pp. 100–105.

[4] M. J. Gans, R. A. Valenzuela, Y.-S. Yeh, and N. Amitay, "Antenna pattern deconvolution for precise incident power density pattern measurement," in *Proc. IEEE 51st Veh. Technol. Conf.*, Tokyo, Japan, May 15–18, 2000, vol. 3, pp. 2532–2535.

[5] J. Li, X.-Z. Li, G.-M. Zhou, and E.-Y. Zhang, "A novel method for estimating the power azimuth spectrum of the wireless channel," *IEEE Antennas Wireless Propag. Lett.*, vol. 5, pp. 11–14, Dec. 2006.

[6] A. F. Molisch, M. Steinbauer, M. Toeltsch, E. Bonek, and R. S. Thoma, "Capacity of MIMO systems based on measured wireless channels," *IEEE J. Sel. Areas Commun.*, vol. 20, pp. 561–569, Apr. 2002.

[7] R. Roy and T. Kailath, "ESPRIT—Estimation of signal parameters via rotational invariance techniques," *IEEE Trans. Acoust., Speech, Signal Process.*, vol. 37, pp. 984–995, Jul. 1989.

[8] B. H. Fleury, M. Tschudin, R. Heddergott, D. Dahlhaus, and K. Ingeman Pedersen, "Channel parameter estimation in mobile radio environments using the SAGE algorithm," *IEEE J. Selected Areas Commun.*, vol. 17, pp. 434–450, Mar. 1999.

[9] M. Landmann, W. A. Kotterman, and R. S. Thomä, "On the influence of data models on estimated angular distributions in channel characterisation," presented at the Proc. Eur. Antennas Propag. Conf., Edinburgh, Scotland, Nov. 11–16, 2007.

[10] M. Nilsson, B. Volcker, and B. Ottersten, "A cluster approach to spatio-temporal channel estimation," in *Proc. IEEE Int. Conf. Acoust., Speech, and Signal Process.*, Istanbul, Turkey, Jun. 5–9, 2000, vol. 5, pp. 2757–2760.

[11] S. S. Chen, D. L. Donoho, and M. A. Saunders, "Atomic decomposition by basis pursuit," *SIAM Rev.*, vol. 43, pp. 129–159, Mar. 2001.

[12] J.-J. Fuchs, "On sparse representations in arbitrary redundant bases," *IEEE Trans. Inf. Theory*, vol. 50, pp. 1341–1344, June 2004.

[13] M. Elad and M. Aharon, "Image denoising via sparse and redundant representations over learned dictionaries," *IEEE Trans. Image Process.*, vol. 15, pp. 3736–3745, Dec. 2006.

[14] J. Wallace, H. Özcelik, M. Herdin, E. Bonek, and M. Jensen, "A diffuse multipath spectrum estimation technique for directional channel modeling," in *Proc. IEEE Intl. Conf. Commun.*, Paris, France, Jun. 20–24, 2004, vol. 6, pp. 3183–3187.

[15] J. Wallace and M. Jensen, "Time-varying MIMO channels: Measurement, analysis, and modeling," *IEEE Trans. Antennas Propag.*, vol. 54, pp. 3265–3273, Nov. 2006.

[16] J. Wallace and B. Maharaj, "Accurate MIMO channel modeling: Correlation tensor vs. directional approaches," in *Proc. IEEE Global Telecomm. Conf.*, Washington, DC, Nov. 26–30, 2007, pp. 3750–3754.

[17] J. B. Andersen and K. I. Pedersen, "Angle-of-arrival statistics for low resolution antennas," *IEEE Trans. Antennas Propag.*, vol. 50, pp. 391–395, Mar. 2002.

[18] A. Richter and R. Thoma, "Joint maximum likelihood estimation of specular paths and distributed diffuse scattering," in *Proc. IEEE 61st Veh. Technol. Conf.*, Stockholm, Sweden, May 30–Jun. 1 2005, vol. 1, pp. 11–15.

[19] S. Mallat and Z. Zhang, "Matching pursuit in a time-frequency dictionary," *IEEE Trans. Signal Process.*, vol. 40, pp. 3397–3415, Dec. 1993.

[20] R. M. Leahy and B. D. Jeffs, "On the design of maximally sparse beamforming arrays," *IEEE Trans. Antennas Propag.*, vol. 39, pp. 1178–1187, Aug. 1991.

[21] J.-J. Fuchs and C. Guillemot, "Fast implementation of a $\ell_\infty - \ell_1$ penalized sparse representations algorithm: Applications in image denoising and coding," in *Conf. Record 41st Asilomar Conf. Signals, Syst. and Comput.*, Pacific Grove, CA, Nov. 4–7, 2007, pp. 508–512.

[22] J.-J. Fuchs, "Some further results on the recovery algorithms," presented at the Proc. Conf. on Signal Process. With Adaptative Sparse Structured Representations (SPARS'05), Rennes, France, Nov. 16–18, 2005.

[23] Q. H. Spencer, B. D. Jeffs, M. A. Jensen, and A. L. Swindlehurst, "Modeling the statistical time and angle of arrival characteristics of an indoor multipath channel," *IEEE J. Sel. Areas Commun.*, vol. 18, pp. 347–360, Mar. 2000.

[24] K. I. Pedersen, P. E. Mogensen, and B. H. Fleury, "Power azimuth spectrum in outdoor environments," *Electron. Lett.*, vol. 33, pp. 1583–1584, Aug. 1997.

[25] J. Czyzyk, S. Mehrotra, M. Wagner, and S. Wright, "PCx User Guide (version 1.1)," Optimization Technology Center, Argonne National Laboratory, Tech. Rep. OTC 96/01, 1997.

[26] J. W. Wallace and M. A. Jensen, "Modeling the indoor MIMO wireless channel," *IEEE Trans. Antennas Propag.*, vol. 50, pp. 591–599, May 2002.

[27] M. Herdin, H. Özcelik, H. Hofstetter, and E. Bonek, "Variation of measured indoor MIMO capacity with receive direction and position at 5.2 GHz," *Electron. Lett.*, vol. 38, pp. 1283–1285, Oct. 10, 2002.

[28] J. Wallace, H. Özcelik, M. Herdin, E. Bonek, and M. Jensen, "Power and complex envelope correlation for modeling measured indoor MIMO channels: A beamforming evaluation," in *Proc. IEEE 58th Veh. Technol. Conf.*, Orlando, FL, Oct. 6–9, 2003, vol. 1, pp. 363–367.

Jon W. Wallace (S'99–M'03) received the B.S. (*summa cum laude*) and Ph.D. degrees in electrical engineering from Brigham Young University (BYU), Provo, UT, in 1997 and 2002, respectively.

From 1995 to 1997, he worked as an Associate of Novell, Inc., Provo. During 1997, he was a Member of Technical Staff for Lucent Technologies, Denver, CO. He received the National Science Foundation Graduate Fellowship in 1998 and worked as a Graduate Research Assistant at BYU until 2002. From 2002 to 2003, he was with the Mobile Communications Group, Vienna University of Technology, Vienna, Austria, pursuing collaborative research in the area of wireless channel measurement and modeling. From 2003 to 2006, he was a Research Associate with the BYU Wireless Communications Laboratory, developing platforms for wideband MIMO channel sounding and real-time space-time coding. He is currently an Assistant Professor of Electrical Engineering at Jacobs University Bremen, Bremen, Germany. His current research interests include wireless channel sounding and modeling, MIMO communications, cognitive radio, and UWB and frequency-agile systems.

Dr. Wallace is serving as an Associate Editor of the IEEE TRANSACTIONS ON ANTENNAS AND PROPAGATION.

Michael A. Jensen (S'93–M'95–SM'01–F'08) received the B.S. (*summa cum laude*) and M.S. degrees in electrical engineering from Brigham Young University (BYU), Provo, UT, in 1990 and 1991, respectively, and the Ph.D. degree in electrical engineering from the University of California, Los Angeles (UCLA), in 1994.

Since 1994, he has been at the Electrical and Computer Engineering Department, BYU where he is currently a Professor and Department Chair. His main research interests include antennas and propagation for personal communications, radar remote sensing, numerical electromagnetics, and optical fiber communications.

Dr. Jensen currently chairs the Joint Meetings Committee for the IEEE Antennas and Propagation Society and is an Associate Editor for the IEEE ANTENNAS AND WIRELESS PROPAGATION LETTERS. He has been an Associate Editor for the IEEE TRANSACTIONS ON ANTENNAS AND PROPAGATION, a member of the society AdCom, and Co-chair and Technical Program Chair for several symposia.